Deformable Adaptive Wall Test Section for Three-Dimensional Wind Tunnel Testing

E. Wedemeyer,* A. Heddergott,* and D. Kuczka*
Deutsche Forschungs- und Versuchsanstalt für Luft- und Raumfahrt e.V, Göttingen, Federal Republic of Germany

To create three-dimensional adaptive wind tunnel walls, a test section was constructed from a thick-walled rubber tube. The new test section with a length of 240 cm and a diameter of 80 cm is installed in the high-speed wind tunnel of DFVLR test facility at Göttingen. The cylindrical walls of the test section can be adapted to interference-free boundary conditions by a set of 64 jacks that are driven by stepping motors. The measurement and evaluation of the wall pressures, the computation of the interference-free wall contour, and the wall adaptation by the 64 jacks are computer controlled and performed automatically. First model tests have demonstrated the achievement of interference-free flow.

Nomenclature

A = total wing area
A_b = body base area
A_T = test section area
c = mean aerodynamic chord
C_D = drag coefficient
C_{Db} = base drag cofficient
C_{Df} = forebody drag coefficient
C_L = lift coefficient
C_m = pitching moment coefficient
c_p = pressure coefficient
D = body diameter
D_T = test section diameter
ℓ = length of body
L = test section length
Ma = Mach number
R = radial distance to the wall
Re = Reynolds number
U_∞ = freestream velocity
u,v = longitudinal, normal component of perturbation velocity
x,r,θ = cylindrical coordinate system
α = angle of attack
β = Prandtl factor $= \sqrt{1-Ma^2}$
η = wall displacement
Φ = flow pertubation potential

Subscripts

i,e = internal, external

I. Introduction

THE need for interference-free wind tunnel data in the high subsonic Mach number range has in recent years inspired the construction of wind tunnel test sections with "adaptive walls," i.e., walls that can be adapted to the streamlines of unconfined flow. In conjunction with such test sections, computer codes have been developed for the calculation of the adapted wall contours. The principle of adaptive or "self-streamlining" walls was first described in publications by Sears[1] and Ferri and Baronti.[2]

Streamlining the walls can be achieved either by deflection of the flexible plates that form the test section walls or by wall ventilation. The latter concept can be realized by dividing the outer wall surface into a number of separated compartments so that the airstream through each compartment can be controlled by variation of the back pressure. A method applied at the AEDC[3] uses variable porosity of the walls with constant pressure in the plenum chamber.

An advantage of the wall ventilation methods is the capability of the porous walls to absorb shock waves. On the other hand, there are disadvantages due to the fact that the flow near the perforated walls is quite inhomogeneous, such that measurement of the flow angle and static pressure cannot be performed at or near the wall. These data, which are required for the wall adaptation procedure, must then be measured inside the flow, which in turn creates great difficulties.

The concept of flexible solid plates for the wall adaptation was realized mainly for two-dimensional flows, especially for the testing of wing sections.[4-8] A remarkable exception is the three-dimensional adaptive test section at the Technical University Berlin[9] with an octagonal test section constructed from eight flexible plates and flexible "scales" between the plates.

The concept introduced in this paper uses a thick-walled rubber tube for the adaptive test section. The cylindrical tube can be deformed by a set of 64 motor-driven jacks to any desired wall contour. The construction of the tubes with a very smooth inner surface, as well as the drilling of pressure holes into the walls, provided no difficulties. The new test section was designed so that it could be installed in the existing DFVLR high-speed wind tunnel at Göttingen (HWG). The HWG (which is described in Ref. 10) is a vacuum storage blowdown tunnel with an open-jet test section of 0.75×0.75 m^2 for subsonic flow and a supersonic test section with an adjustable nozzle. In its new mode of operation, the square nozzle and contraction section are replaced by the rubber tube test section and a new nozzle that connects the cylindrical test section with the rectangular settling chamber.

A detailed description of the rubber tube test section is given in Sec. II. Section III presents a method for the computation of the three-dimensional adapted wall contour. Finally, in Sec. IV, the first results of model tests are presented and compared with interference-free reference data.

II. Description of the Rubber Tube Test Section

For two-dimensional flows past wing sections, etc., wall adaptation has been achieved by use of flexible plates for the

Received March 16, 1985; revision received July 15, 1985.

*Institut für Experimentelle Strömungsmechanik.

upper and lower test section walls. For general three-dimensional flows, the walls must be three-dimensionally deformable (i.e., flexible and stretchable) in order to be adjustable to the streamlines of the unconfined flow.

To create the three-dimensional adaptive walls, the test section was constructed from a thick-walled rubber tube. The new test section, having a length of 240 cm and a circular cross section of 80 cm diameter was installed in the existing blowdown wind tunnel of the DFVLR, Göttingen. Figures 1 and 2 are schematic drawings of the DFVLR blowdown tunnel and the new test section. A photograph of the test section before installation is shown in Fig. 3.

A circular cross section was chosen for the rubber tube, as it was easy to manufacture and gave the most uniform load distribution on the supporting jacks.

The rubber tube is flanged at the upstream end onto the circular nozzle. The other (free) end extends to the bell-shaped collector. The tube is supported and can be deformed by a set of 64 jacks that are connected to a rigid frame around the test section. The jacks are driven by stepping motors. At each of the eight cross sections, eight jacks are mounted over the circumferences with equal angular distances between every two adjacent jacks. The hinged connection of the jacks allows for a small lateral displacement. Each jack acts via four support points on the rubber wall so that the deforming force is more evenly distributed over the surface. The supports are vulcanized into the rubber wall. The short distances between the adjacent support points and the relatively large wall thickness of 6 cm assure that the wall is sufficiently stiff and that it remains fairly smooth (i.e., free from detrimental waviness) after deformation.

The holes for wall pressure measurements are located at the ¼ and ¾ position between the support points in longitudinal direction and halfway between the supports in the circumferential direction (Fig. 2). These have been calculated as positions of minimum error due to the wall waviness effects.

Wall pressures and displacement are measured at the 64 positions of the jacks. In addition to the recordings of the stepping motors, 64 potentiometers are used to measure the wall displacement. The measurement of the wall data, wall adaptation, and model testing is performed fully automatically.

A psi pressure transducer and acquisition system is used for pressure distributions on the test section walls as well as for wind tunnel models. The system allows up to 14,000 pressure recordings per second with an accuracy of about 0.5×10^{-3} bar (0.725×10^{-2} psi).

A microcomputer PDP 11/23 PLUS for data reduction and control of the wall adaptation and test procedure and a graphic terminal VT 100 RG are available at the wind tunnel. The final evaluation of the test results, storage of data, and the computation of wall contours are performed at the central computer. Figure 4 shows a control diagram of the test section.

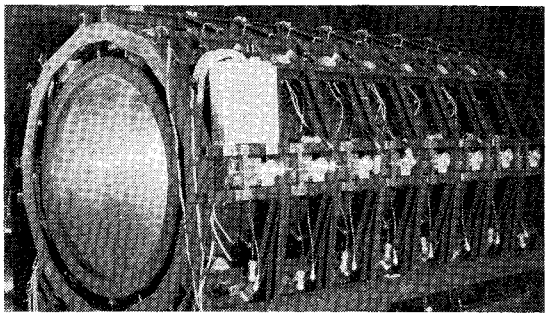

Fig. 3 Adaptive rubber tube test section.

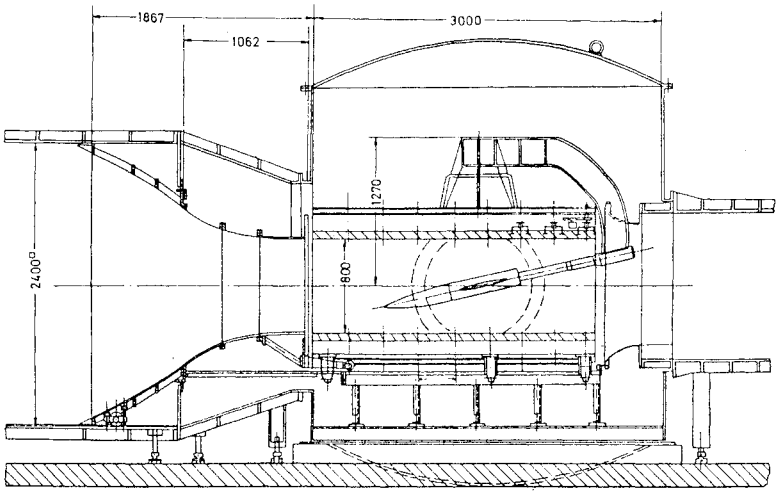

Fig. 1 High-speed wind tunnel with deformable adaptive test section [$Ma = 0.4\text{-}1.0$, $A_T = 0.5026$ m^2 (0.8 m diameter), 45 s maximum operating time, 11.5 contraction ratio].

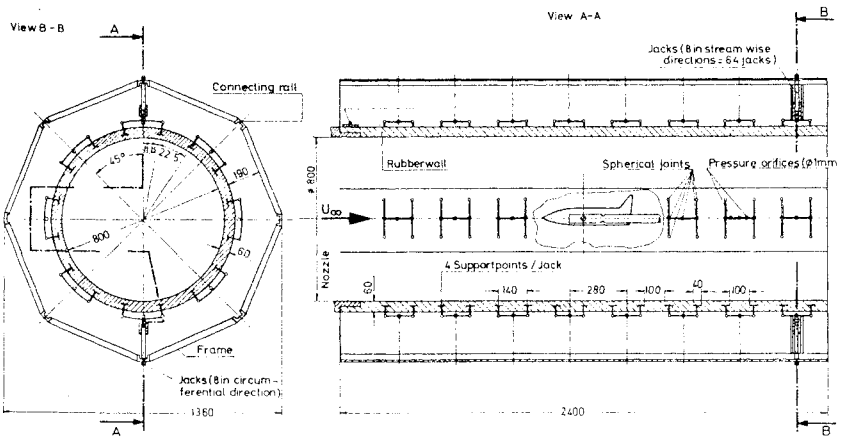

Fig. 2 Adaptive rubber tube test section for 0.8 m high-speed wind tunnel at DFVLR Göttingen.

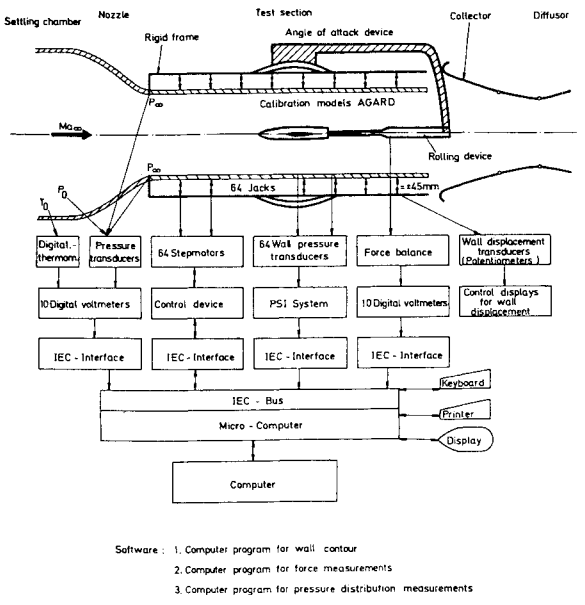

Fig. 4 Control diagram of deformable adaptive test section.

III. Wall Adaptation Scheme

The principle of wall adaptation, as described by Sears,[1] requires the measurement of two independent flow variables at the wall, e.g., the normal v and tangential u velocity components. An equivalent pair of flow variables are the wall pressure p and wall displacement η.

For the rubber wall test section, the wall pressure is measured in a first tunnel run. The measured pressures and the initial wall displacement (which can, but need not, be zero) are recorded and used as input for the calculation of the adapted wall contour.

For a given wall contour, a fictitious "external flow" is defined (Fig. 5) as a potential flow that is tangential to the wall contour and passes into undisturbed parallel flow at infinity. The external flow can be computed on the basis of potential flow theory. The computed external flow is, in general, not a physical continuation of the internal flow unless the wall pressure is continuous (i.e., the measured pressure $p_{(i)}$ at the inside of the wall agrees with the computed external wall pressure $p_{(e)}$ at every point on the wall surface). The mathematical problem of wall adaptation consists of finding a wall contour for which the pressure is continuous across the wall, i.e., $p_{(i)} = p_{(e)}$. Usually, this problem is solved iteratively: the wall is displaced so as to decrease the pressure jump $(p_{(i)} - p_{(e)})$. For the displaced wall, a new pressure distribution $p_{(i)}$ is measured and compared with the new theoretical distribution of $p_{(e)}$, etc.

Under certain conditions, the wall adaptation can be achieved within one iteration step. The one-step method used for the rubber wall test section is described in the following paragraphs.

The method of wall adaptation described here is based on the assumption that the flow is subsonic near the test section walls and that the wall deflections are sufficiently small so that flow disturbances due to these wall deflections can be described by the linearized potential equation. Under this assumption, the flow induced by the wall deflections can be superimposed on the flow induced by the model.

Then, after wall deflection, the resulting flow variables on the inside of the wall must be equal to the flow variables on the outside. This condition leads to a set of linear equations for the wall deflection. In cases where supersonic pockets extend up to the test section wall, the proposition of linearized flow theory is certainly incorrect and a more elaborate iterative method becomes necessary for the adaptation of the wall.

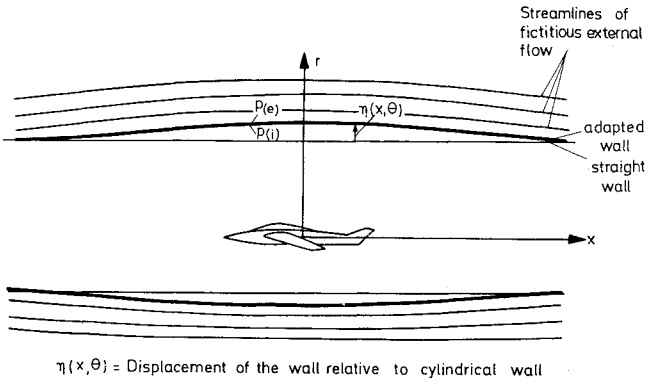

Fig. 5 Principle of adaptive walls.

The one-step method, whenever it is applicable, is preferable because it computes the adapted wall contour in one iteration step and thus saves tunnel running time.

A cylindrical coordinate system (x, r, θ) is used with velocity components (u, v, w), respectively. The wall displacement is denoted by $\eta(x, \theta)$, i.e., the displaced wall has a distance from the centerline, $R = R_0 + \eta(x, \theta)$. See Fig. 5. The initial wall displacement is denoted by $\eta_0(x, \theta)$. η_0 can, for example, be identically zero. It is, however, useful to choose for η_0 the wall setting of the previous measurement at a neighboring Mach number or angle of incidence.

For the initial wall setting η_0, the interior flow about the model can be described (at least in the wall region) by a perturbation potential $\Phi_0(x, r, \theta)$. Φ_0 is unknown, but the velocity components at the wall $u_0 = (\partial\Phi_0/\partial x)_R$ and $v_0 = (\partial\Phi_0/\partial r)_R$ are known by measuring the wall pressure $(\Delta p_0 = -\rho U_\infty u_0)$ and the wall displacement $(v_0 = U_\infty \mathrm{d}\eta_0/\mathrm{d}x)$.

An additional wall displacement $\Delta\eta = \eta_1 - \eta_0$ generates an additional perturbation potential $\varphi_{(i)}$. The perturbation potential for the outer flow may be denoted by $\varphi_{(e)}$, $\varphi_{(i)}$, and $\varphi_{(e)}$ are solutions of the linearized potential equation,

$$\beta^2\varphi_{xx} + \varphi_{rr} + \frac{1}{r}\varphi_r + \frac{1}{r^2}\varphi_{\theta\theta} = 0$$

Taking advantage of the cylindrical geometry of the test section, we can expand $\varphi_{(i)}$ and $\varphi_{(e)}$ in a Fourier series. The total perturbation potential for the internal flow can then be written as

$$\Phi_{(i)} = \Phi_0 + U_\infty \sum_{n,k} a_{n,k} I_n(\beta kr) e^{i(n\theta + kx)} \tag{1}$$

For the fictitious external flow, we assume a perturbation potential,

$$\Phi_{(e)} = U_\infty \sum_{n.k} b_{n,k} K_n(\beta kr) e^{i(n\theta + kx)} \tag{2}$$

where I_n and K_n are modified Bessel functions. Since the perturbation due to the wall displacement must have no singularities, only the I_n can be used for the internal flow [Eq. (1)] and only the K_n can be used for the external flow as only the K_n are bounded for $r \to \infty$.

The coefficients $a_{n,k}$ and $b_{n,k}$ are now determined by the conditions

$$v_{(i)} = v_{(e)} \quad \text{and} \quad u_{(i)} = u_{(e)}$$

with

$$v_{(i)} = \left(\frac{\partial\Phi_{(i)}}{\partial r}\right)_R ; \qquad v_{(e)} = \left(\frac{\partial\Phi_{(e)}}{\partial r}\right)_R$$

$$u_{(i)} = \left(\frac{\partial\Phi_{(i)}}{\partial x}\right)_R ; \qquad u_{(e)} = \left(\frac{\partial\Phi_{(e)}}{\partial x}\right)_R$$

With Eqs. (1) and (2), we get

$$v_{(i)} = v_0 + U_\infty \sum_{n,k} a_{n,k} I_n'(\beta kR) \cdot \beta k e^{i(n\theta + kx)} \tag{3}$$

$$v_{(e)} = U_\infty \sum_{n,k} b_{n,k} K_n'(\beta kR) \cdot \beta k e^{i(n\theta + kx)} \tag{4}$$

Integration of Eqs. (3) and (4) results in

$$\eta_{1(i)} = \eta_0 + \sum_{n,k} \frac{\beta}{i} a_{n,k} I_n'(\beta kR) e^{i(n\theta + kx)} \tag{5}$$

$$\eta_{1(e)} = \sum_{n,k} \frac{\beta}{i} b_{n,k} K_n'(\beta kr) e^{i(n\theta + kx)} \tag{6}$$

For the tangential velocity components, Eqs. (1) and (2) give

$$u_{(i)} = u_0 + U_\infty \sum_{n,k} a_{n,k} ik I_n(\beta kR) e^{i(n\theta + kx)} \tag{7}$$

$$u_{(e)} = U_\infty \sum_{n,k} b_{n,k} ik K_n(\beta kR) e^{i(n\theta + kx)} \tag{8}$$

From $\eta_{(i)} = \eta_{(e)}$ and $u_{(i)} = u_{(e)}$, we obtain with Eqs. (5-8)

$$\eta_0 = \sum_{n,k} \frac{\beta}{i} (b_{n,k} K_n' - a_{n,k} I_n') e^{i(n\theta + kx)} \tag{9}$$

$$\frac{u_0}{U_\infty} = \sum_{n,k} ik (b_{n,k} K_n - a_{n,k} I_n) e^{i(n\theta + kx)} \tag{10}$$

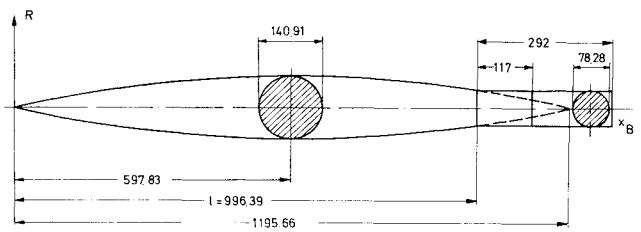

Fig. 6 FFA calibration model (parabolic spindle) for pressure measurements (blockage ratio = 3.1%).

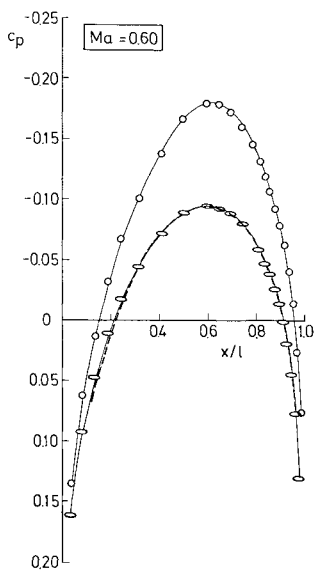

Fig. 7 Pressure distribution for FFA model: ○ not adapted, ○ adapted, --- theory, $\alpha = 0$ deg.

Fourier transformation of Eqs. (9) and (10) gives

$$\frac{\beta}{i}(b_{n,k} K_n' - a_{n,k} I_n') = \frac{1}{(2\pi)^2} \int\int \eta_0 e^{-i(n\theta + kx)} d\theta dx \tag{11}$$

$$ik(b_{n,k} K_n - a_{n,k} I_n) = \frac{1}{(2\pi)^2} \int\int \frac{u_0}{U_\infty} e^{-i(n\theta + kx)} d\theta dx \tag{12}$$

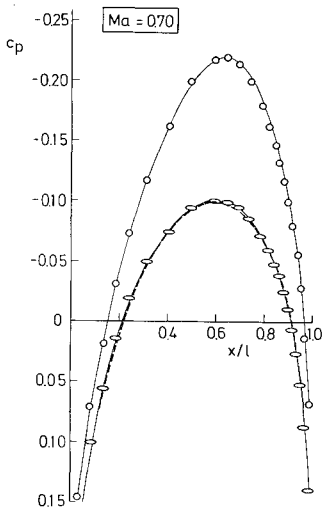

Fig. 8 Pressure distribution for FFA model: ○ not adapted, ○ adapted, --- theory, $\alpha = 0$ deg.

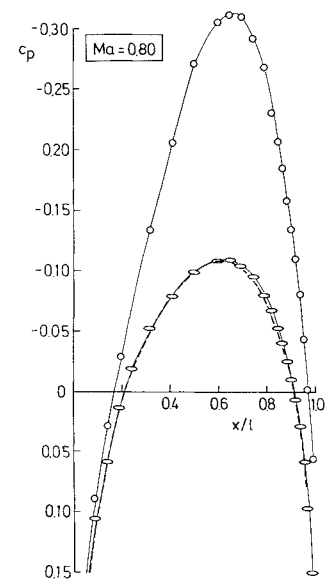

Fig. 9 Pressure distribution for FFA model: ○ not adapted, ○ adapted, --- theory, $\alpha = 0$ deg.

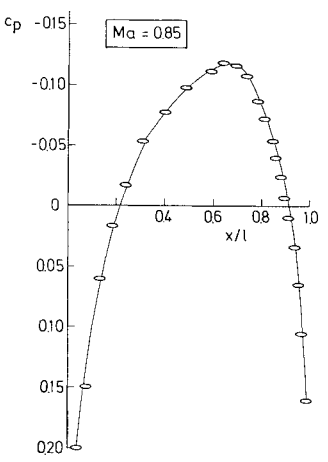

Fig. 10 Pressure distribution for FFA model: ○ adapted, $\alpha = 0$ deg.

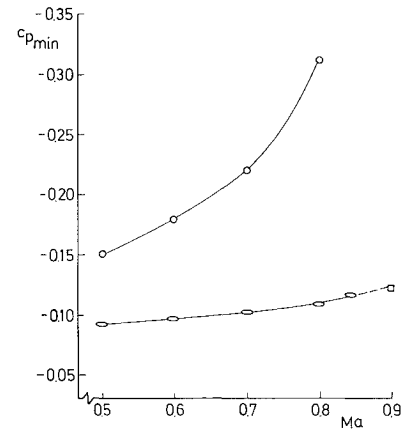

Fig. 11 Minimum c_p values: ○ not adapted, ⊂ adapted, □ FAA theory.

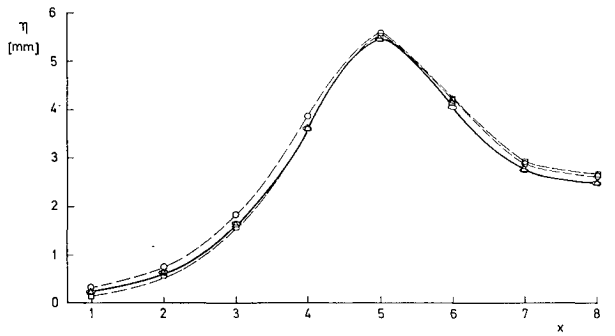

Fig. 12 Adapted wall contour for FFA model (blockage = 3.1%): $\alpha = 0$ deg, □ first ○ second, △ third, and ⊂ fourth iterations.

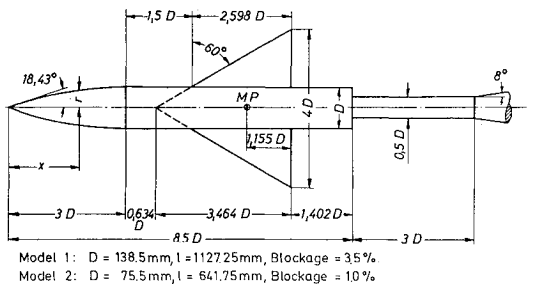

Fig. 13 AGARD calibration model B.

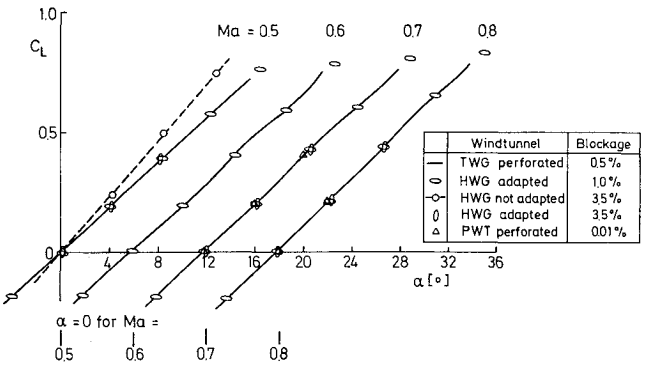

Fig. 14 C_L vs α for AGARD calibration models.

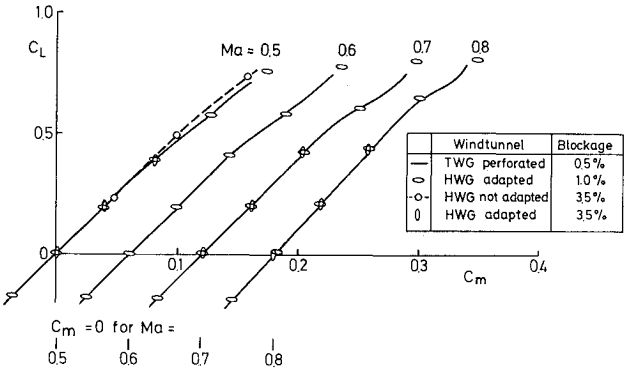

Fig. 15 C_L vs C_m for AGARD calibration models.

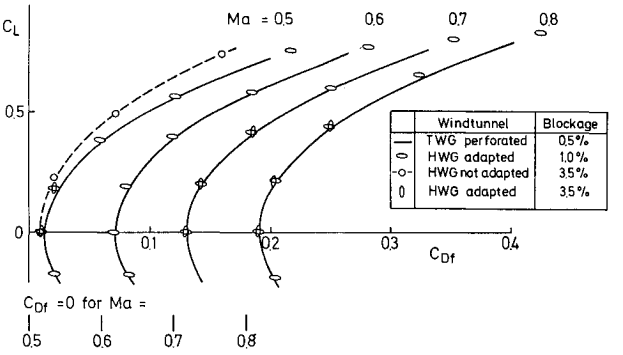

Fig. 16 C_L vs C_{Df} for AGARD calibration models.

Table 1 General data on models and facilities

Symbol in Figs.	Institute facility	Test section: Size	Walls	Open, %	Slot depth	Blockage, %	Reynolds no. ($\times 10^{-6}$)
		FFA model[a]					
○	DFVLR/HWG adapted test section[b]	Diam 0.8 m	Cylindrical	0	—	3.1	12.9[c]
⊂	DFVLR/HWG adapted test section[b]	Diam 0.8 m	Adapted	0	—	3.1	12.9
□	FFA/transonic wind tunnel[12,b]	0.89×0.89 m^2	Slotted	9.2	18.9	2.2	9.7
		AGARD calibrated model B[d]					
○	DFVLR/HWG adaptive test section	Diam 0.8 m	Cylindrical	0	—	3.5	2.5-4.5[c]
0	DFVLR/HWG adaptive test section	Diam 0.8 m	Adapted	0	—	3.5	2.5-4.5
⊂	DFVLR/HWG adaptive test section[6]	Diam 0.8 m	Adapted	0	—	1.0	1.4-4.5
—	DFVLR/TWG (transonic wind tunnel)[13,b]	1.0×1.0 m^2	4 perforated	6		0.5	1.6-2.6
△	AEDC/transonic model tunnel	0.31×0.31 m^2	4 perforated	6	—	2.5	1.6-2.0
◇	AEDC/PWT transonic circuit[14]	4.88×4.88 m^2	4 perforated	6	—	0.01	0.7-1.2
▽	AEDC/PWT transonic circuit[14]	4.88×4.88 m^2	4 perforated	6	—	1.15	8.5-1.2
×	NACA	Free flight					1.0-2.7

[a]Pressure measurement. [b]Same model, transition free. [c]Based on L. [d]Force measurements. [e]Based on $\ell\mu$.

Finally, Eqs. (11) and (12) can be solved for $a_{n,k}$ and $b_{n,k}$,

$$b_{nk} = \left[I_n' \int\int \frac{u_0}{U_\infty} e^{-i(n\theta+kx)} d\theta dx + \frac{k}{\beta} I_n \int\int \eta_0 e^{-i(n\theta+kx)} d\theta dx \right] \div ik(2\pi)^2 (I_n' K_n - I_n K_n') \quad (13)$$

Inserting $b_{n,k}$ into Eq. (6) gives the wall displacement $\eta_1 = \eta_{1(e)}$,

$$\eta_1 = \frac{\beta}{i} \sum b_{n,k} K_n'(\beta k R) e^{i(n\theta+kx)} dx \quad (14)$$

The method described above requires that the perturbation potential be periodic in x so that it can be expanded into a Fourier series [Eq. (1)]. The length of the period may be chosen to be two or four times the test section length. To alleviate the requirement of periodicity, it is suitable to extend the Fourier series using terms varying linearly with x. A computational procedure based on this assumption is described in Ref. 11.

IV. Model Tests

A number of model tests have been performed in order to demonstrate the capability of the adapted test section to produce interference-free data and to investigate its limitations. An overlook of the DFVLR model tests and reference tests at other facilities is shown in Table 1. In this section, a few remarks are made about the tunnel calibration and the results of the model tests (pressure distribution and force measurements) are discussed.

Calibration of the Empty Test Section

To compensate for the displacement effects of the wall boundary layer, the walls must be adjusted to be slightly divergent. In principle, this is easy to attain for the rubber wall test section. A computer program, similar in structure to the program for the wall adaptation, was used to adapt the walls to the condition of constant undisturbed pressure. It was due to an unexpected test experience that errors in the pressure measurement caused by faulty pressure holes had a striking effect on the resulting wall contour. At first, a provisional averaging method was used to overcome the difficulties. It appears, however, to be desirable to calibrate all of the pressure taps, a task now underway.

The wall adjustment that gives zero pressure coefficients for the empty test section is taken as the reference point and is referred to as a "not-adapted" or "aerodynamically straight" wall.

Pressure Distribution Measurements on FFA Calibration Model

The FFA calibration model[12] used for pressure distribution tests has a blockage ratio of 3.1% in the not-adapted test section, so large wall interference effects can be expected. Figure 6 shows the model that is a parabolic spindle supported by a cylindrical afterbody. Figures 7-9 give the results of pressure measurements for adapted and not-adapted walls at Mach numbers of 0.6-0.8. For $Ma = 0.85$, only the data for adapted walls are shown (Fig. 10) as the not-adapted test section was choked. The strong wall interference for straight walls is completely reduced after the wall adaptation, as shown by comparison with theoretical interference-free data. Unfortunately, no interference-free experimental data were availabe for comparison in the Mach number range tested.

The theoretical data are based on linearized theory and may be faulty for $Ma \geq 0.8$. A partial comparison with experimental data is shown in Fig. 11 where the minimum c_p values are plotted vs Mach number. The extrapolation of the curve to $Ma = 0.9$ compares well with a theoretical value computed at FFA.

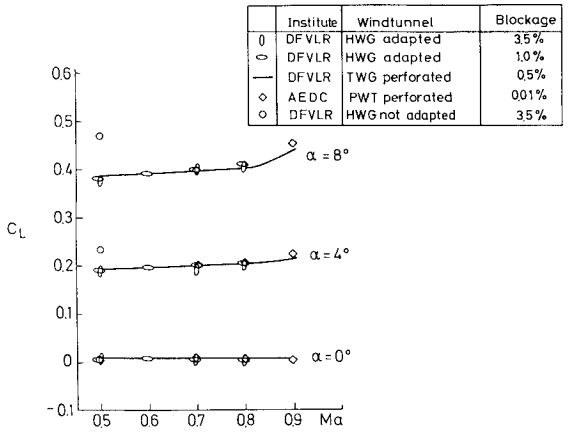

Fig. 17 C_L vs Ma for AGARD calibration models.

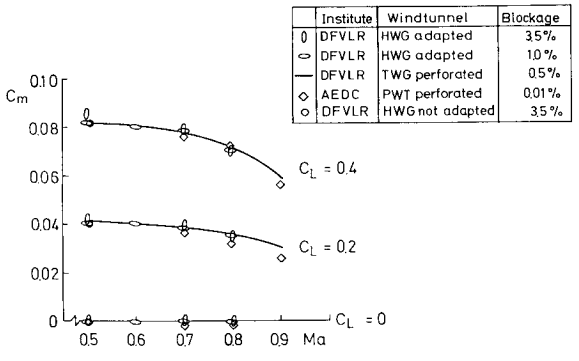

Fig. 18 C_m vs Ma for AGARD calibration models.

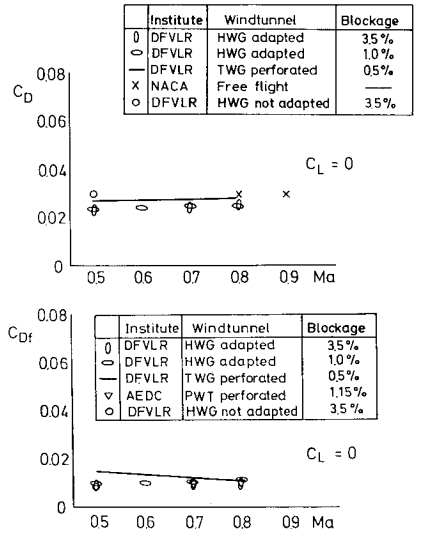

Fig. 19 C_D vs Ma and C_{Df} vs Ma for AGARD calibration models.

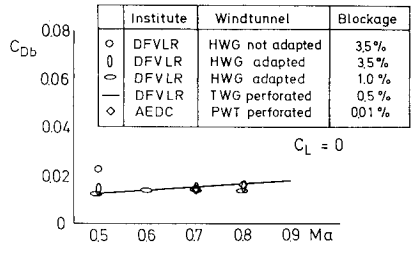

Fig. 20 C_{Db} vs Ma for AGARD calibration models.

Figure 12 shows the axisymmetric wall displacement for the FFA model after the wall has been adapted. The practicability of the one-step iteration method is clearly demonstrated as iterations 2-4 did not yield any improvement.

Force Measurements on Two AGARD Calibration Models

Force measurements were made on two AGARD calibration models of different size with tunnel blockage ratios of 1 and 3.5%, respectively. The experimental data are compared with data of other wind tunnels,[13] which are considered as interference-free reference data as they were obtained in slotted or perforated test sections with very low blockage ratios.

The relative dimensions of the AGARD calibration model are shown in Fig. 13. Figures 14-20 show the experimental results for the force coefficients C_L, C_m, and C_D and the forebody and base drag C_{Df} and C_{DB}. The agreement with the interference-free reference data is remarkably good even for the large model (with 3.5% blockage ratio and 26% wing surface to tunnel cross-sectional area). To give an impression of the wall interferences, data for the not-adapted wall are shown in the diagrams for $Ma = 0.5$. For large Mach numbers, the not-adapted test section is again choked.

In Fig. 19, drag and forebody drag data are plotted vs Mach number. The reference data from the TWG perforated test section with 0.5% blockage are somewhat larger than our data. It is very likely that these reference data are still influenced by wall interference effects. Also, the free-flight data for C_D are larger, which is plausible because the effect of the sting support on the model is to reduce the drag coefficient of the wind tunnel data compared with free-flight data.

The base drag data shown in Fig. 20 are again in good agreement with all of the reference data. The base drag in the not-adapted test section for the large model is very high, an effect that can be explained by the wake-induced axial pressure gradient.

V. Conclusions

The concept of the rubber tube test section for three-dimensional adaptive wall wind tunnel testing proved to be very successful. The model tests have demonstrated that interference-free flow can be achieved.

The measurement of wall pressures needs further attention. An improvement is expected from the calibration of the individual pressure orifices.

Acknowledgment

The authors wish to acknowledge the invaluable support received by personnel of the wind tunnel devision (HA-WK) and the electronics group (TB-DT) of the DFVLR Göttingen.

References

[1]Sears, W.R., "Self-Correcting Wind Tunnels," *Aeronautical Journal*, Vol. 78, Feb.-March 1974.

[2]Ferri, A. and Baronti, P., "A Method for Transonic Wind Tunnel Corrections," *AIAA Journal*, Vol. 11, Jan. 1973.

[3]Parker Jr., R.L. and Erickson, J.C. Jr., "Development of a Three-Dimensional Adaptive Wall Test Section with Perforated Walls," AGARD CP-335, May 1983.

[4]Chevallier, J.P., "Soufflerie transsonique a parois auto-adaptable," ONERA, TP 1975-119, 1975.

[5]Ganzer, U., "Windkanäle mit adaptiven Wänden zur Beseitigung von Wandinterferenzen," *Zeitschrift fuer Flugwissenschaften Weltraumforsch.*, Vol. 3, No. 2, 1979.

[6]Chevallier, J.P., Mignosi, A., Archembaud, J.P., and Seraudie, A., "Parois adaptable a T2," Recherche Aerospatiale, No. 4, 1983.

[7]Schairer, E.T. and Mendoza, J.P., "Adaptive-Wall Tunnel Research at Ames Research Center," AGARD CP-335, May 1982.

[8]Goodyer, M.J., and Wolf, S.W.D., "Development of a Self-Streamlining Flexible Walled Transonic Test Section," *AIAA Journal*, Vol. 20, Feb. 1982.

[9]Ganzer, U., "On the Use of Adaptive Walls for Transonic Wind Tunnel Testing," AGARD CP-335, May 1982.

[10]Ludwieg, H. and Hottner, T., "Hochgeschwindigkeitskanal der Aerodynamischen Versuchsanstalt Göttingen," *Zeitschrift fuer Flugwissenschaften*, Vol. 7, No. 10, 1959.

[11]Müller-Wichards, D. and Gülzow, V., "Ein Potentialtheoretisches Näherungsverfahren zur Berechnung der Kontur einer adaptiven Messtrecke," DFVLR-Bericht IB 262-84 R 01.

[12]Berndt, S.B., "Flow Properties of Slotted-Wall Test Sections," AGARD CP-335, May 1982.

[13]Schneider, W. "Drei-Komponentenmessungen an den AGARD-Eichmodellen B und C im Transsonischen Windkanal der AVA," DLR-FB 66-10, Feb. 1966.

[14]"A Review of Measurements on AGARD Calibration Models," AGARDograph 64, 1961.